Article

Gd(OH)₃ and Co-Doped Gd(OH)₃ for Photocatalytic Degradation of 4-Nitrophenol and Brilliant Green

Shaidatul Najihah Matussin, Fazlurrahman Khan, Mohammad Hilni Harunsani, Young-Mog Kim, and Mohammad Mansoob Khan*

Cite This: ACS Omega 2025, 10, 10183−10192

Read Online

ACCESS | Metrics & More | Article Recommendations | SI Supporting Information

ABSTRACT: The microwave-assisted synthesis method was used to synthesize gadolinium hydroxide nanorods (GH NRs) and 4−12% cobalt-doped gadolinium hydroxide nanorods (4CGH, 8CGH, and 12CGH NRs). X-ray diffraction confirmed that the GH NRs and CGH NRs are in the hexagonal phase with average crystallite sizes between 17 and 36 nm. Raman and FT-IR spectra confirmed the presence of vibrational modes of GH and CGH. The influence of Co doping was observed in the reduction of the band gap energy from 5.00 to 4.29 eV. TEM images showed nanorods of GH and CGH and that the particle size was increased upon doping with Co^{2+}. Photocatalytic degradations of 4-nitrophenol (4-NP) and brilliant green (BG) were carried out under UV light irradiation in which 8CGH NRs had the highest photocatalytic degradation of BG (90%) with a kinetic rate of 0.4636 h^{-1}, while 12CGH NRs showed the highest photocatalytic degradation of 4-NP (78%) with a kinetic rate of 0.2426 h^{-1}. Both photocatalytic degradation activities using the synthesized materials followed a pseudo-first-order kinetic reaction. Therefore, GH and CGH NRs demonstrated efficient application under UV light irradiation.
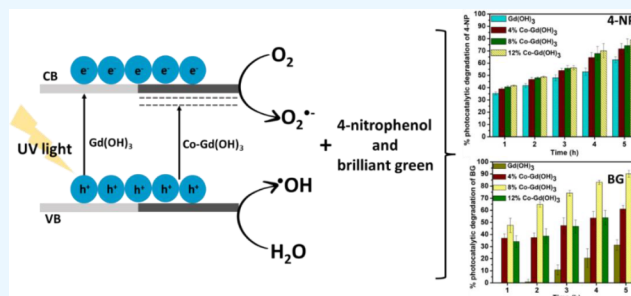
1. INTRODUCTION

Nanoparticles (NPs) are ultrasmall particles with sizes between 1 and 100 nm and can have enhanced chemical or physical properties compared to their bulk equivalents.[1,2] Transition metal oxide NPs have various uses such as in catalysis, sensors, magnetics, electronics, and optics because of their different valence states, high surface areas, and varied electronic structures.[3−5] In addition, the nanoparticle size and morphology can have a major effect on the physiochemical properties of the NPs. Thus, the size and morphology of the NPs should be taken into consideration.[6,7]

Rare-earth elements are a group of 15 lanthanide elements having distinctive 4f electron configurations, ranging from lanthanum to lutetium.[8−10] Rare-earth elements can have a variety of valences, with trivalent rare-earth ions being the most prevalent. Owing to their lack of involvement in chemical bonding, the unpaired 4f electrons of trivalent rare-earth ions exhibit special energy-storage characteristics.[11,12] Furthermore, because of their composite's exceptional physical and chemical qualities, unique unpaired 4f electronic configuration, and controlled structure, rare-earth elements have increasingly drawn the interest of researchers.[11,12] The potential applications of these promising materials in luminescent and biomedical devices, optoelectronics, sensors, detectors, catalysts, and other fields have been studied. Furthermore, rare-earth compounds are primarily used as functional materials and fluorescent markers for biosensing.[8,13,14] Rare-earth hydroxides

among others are important materials that have been fabricated using different techniques, namely, hydrothermal, precipitation, microwave-assisted, sonochemical, etc.[15−19]

Gadolinium ions (Gd^{3+}) have a maximum number of seven 4f unpaired electrons and an ionic radius of 0.094 nm.[20] Gd compounds, particularly, gadolinium hydroxide (GH), are mainly used as MRI contrast agents and have extended to other applications such as CT contrast agents, photocatalysis, and drug delivery.[21−24] GH has been produced at various particle sizes.[19,25−28] For instance, a hydrothermal reaction was used by Du et al. to synthesize GH nanorods (NRs).[26] After 24 h of synthesis at 180 °C, the material that was produced was shown to resemble a rod with a mean length of 90 nm and a diameter of 20 nm. In a comparable approach, Chen et al. carried out the synthesis for 10 h at 120 °C. A rod-like GH was produced, with dimensions of 200−500 nm for the length and 100−200 nm for the diameter. On the other hand, the precipitation method was utilized as reported by Singh et al. to synthesize GH nanoclusters.[29] A cluster of rod-like structures with an average length between 30 and 40 nm was produced.
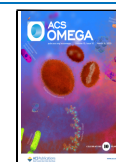
However, limited reports are available for the synthesis of metal-doped GH. Eu-doped GH was synthesized using a precipitation method, which produced a hexagonal microprism of Eu-doped GH.[30] Moreover, the rod-like morphology of Fe-doped GH nanorods was obtained using a hydrothermal method.[31]

Colored organic pollutants such as dyes can consist of nonbiodegradable, highly poisonous, and colored pigments, and these pollutants are reported to be widely present in industrial wastewater.[32,33] Dyes can pollute various aquatic environments and can affect the visible appearance of the water even at relatively low concentrations.[34] Moreover, dyes are considered harmful to living organisms.[34] Therefore, it is essential to remove them from main water sources or wastewater. Furthermore, in nature, uncolored pollutants like p-nitrophenol (4-NP) are persistent, making it challenging for 4-NP to mineralize or degrade in large quantities. Its high solubility and stability also contribute to adverse environmental and health effects. Exposure to 4-NP may cause health problems in both humans and animals, including headaches, vomiting, and organ dysfunction.[35] GH has shown particular promise as a photocatalyst. For instance, GH NRs were used to degrade Congo red.[36] It was reported that the photocatalytic degradation of Congo red was almost 100% within 1400 min. Therefore, GH and its doped GH have the potential to degrade colored and noncolored organic pollutants.

In this work, GH and Co−Gd(OH)$_3$ (CGH) NRs were prepared by using a microwave-assisted synthesis method. The microwave-assisted method was used in this study as it can accelerate chemical reactions by rapidly providing energy to the reaction mixture, which significantly shortens the reaction times compared to conventional methods.[37] Moreover, the rapid and uniform heating provided by microwaves can improve the efficiency of the synthesis reactions by promoting faster kinetics and higher yields. Apart from that, it allows for precise control over reaction conditions, such as temperature and pressure, for obtaining products with desired properties. In a previous study, the synthesis of GH and Ni-GH NRs using a microwave-assisted method was reported.[38] This work is an extension of the previous work, in order to understand the effect of Co doping on the optical and structural properties of Gd(OH)$_3$.[38] However, to the best of the authors' knowledge, there are no current reports on the microwave-assisted synthesis of CGH NRs that have been documented. Different techniques were used to investigate the structure, morphology, and optical properties of the GH and CGH NRs. Additionally, the photocatalytic performance of the synthesized materials under UV light irradiation was also investigated.

2. EXPERIMENTAL PROCEDURE

2.1. Microwave-Assisted Synthesis of GH and CGH NRs.
GH NRs were synthesized using a microwave-assisted method as reported.[38] Briefly, 15 mL of a 0.05 M Gd(NO$_3$)$_3$·6H$_2$O (99%, Sigma-Aldrich) solution was prepared in a microwave vessel. Then, 2.4 mL of 1 M NaOH (99%, Merck) was added dropwise to the solution. The prepared solution was then placed in an Anton Paar Monowave 400 microwave reactor, where the temperature was gradually raised from ambient temperature to 90 °C and eventually to 180 °C. The temperature was kept at 850 W microwave radiation for 15 min. Following the formation of the precipitate, it was centrifuged, washed with distilled water, and then placed in a drying oven at 80 °C.

CGH NRs were similarly synthesized by using the previously described procedure. CoCl$_2$·6H$_2$O (99%, Sigma-Aldrich) was combined with Gd(NO$_3$)$_3$·6H$_2$O to produce 4, 8, and 12CGH NRs (Table 1). The samples were coded as 4CGH, 8CGH, and 12CGH for 4, 8, and 12% Co−Gd(OH)$_3$, respectively.

Table 1. Amount of Gd(NO$_3$)$_3$·6H$_2$O and CoCl$_2$·6H$_2$O Used to Synthesize GH and CGH NRs

Materials	Amount of Gd(NO$_3$)$_3$·6H$_2$O (g)	Amount of CoCl$_2$·6H$_2$O (g)
GH NRs	0.3385	-
4CGH NRs	0.3250	0.0135
8CGH NRs	0.3114	0.0271
12CGH NRs	0.2979	0.0406

2.2. Characterizations.
The XRD, FTIR, Raman, and XPS studies of GH and CGH NRs were investigated using an X-ray diffractometer from Shimadzu XRD-7000 with Cu Kα radiation (λ = 1.5418 Å) and a step size of 0.026°; an FTIR Spectrophotometer from Shimadzu IRPrestige-21 in the range of 450 to 4000 cm^{-1}; a Raman spectrometer from NRS-5100, JASCO, at a laser wavelength of 785 nm at a maximum resolution of 1 cm^{-1} in the range of 50−4000 cm^{-1}; and an X-ray photoelectron spectrometer from Kratos Analytical, AXIS Nova, with 225 W X-ray power from the 286.69 to 1486.69 eV scan range for 1 × 1 cm analysis area, respectively. Furthermore, the optical band gap energy of GH and CGH NRs was investigated by using a UV−vis DRS spectrometer from Shimadzu, UV-2600. Field emission transmission electron microscopy (FE-TEM) and selected area electron diffraction (SAED) using a JEM-F200 (JEOL Ltd., Tokyo, Japan) instrument with an ultrathin carbon film-supported copper grid at 200 kV were used to evaluate the morphology.

2.3. UV Light-Assisted Photocatalytic Degradation of 4-NP and BG.
Photocatalytic degradation of 4-NP (99%, Sigma-Aldrich) using GH and 4, 8, and 12CGH NRs under UV light irradiation (mercury lamp, 300 W, 220 ± 20 V, λ = 365 nm) was investigated. A Toption (TOPT-V) photochemical reactor having a 300 W UV lamp was used to perform the photocatalytic activities, and a UV−visible spectrophotometer (Shimadzu UV-1900, Japan) was used to measure the absorbance of the pollutants.

Small dosages of GH and 4, 8, and 12CGH NRs (10 mg) were mixed in a separate tube containing 50 mL of 10 ppm of 4-NP solution. The sample mixture was sonicated for 3 min before it was stirred for an additional 3 min in the dark. The reaction tubes were then exposed to 300 W UV light for 5 h, in which the absorbance of the treated 4-NP solution was measured every hour. The progress of the photocatalytic activity was obtained using eq 1.

In a similar approach, GH and 4, 8, and 12CGH NRs were also employed in the photocatalytic degradation of 10 ppm of BG dye under 300 W UV light irradiation. The photocatalysis procedure was the same as that previously explained. In short, 50 mL of 10 ppm of aqueous BG solution was combined with 20 mg of GH and 4, 8, and 12CGH NRs. After 3 min of sonication, the sample was agitated for an additional 3 min in the dark. The reaction tubes were subjected to a 5-h UV light exposure. The progress of the BG degradation was monitored, and the percentage degradation was also estimated using eq 1.
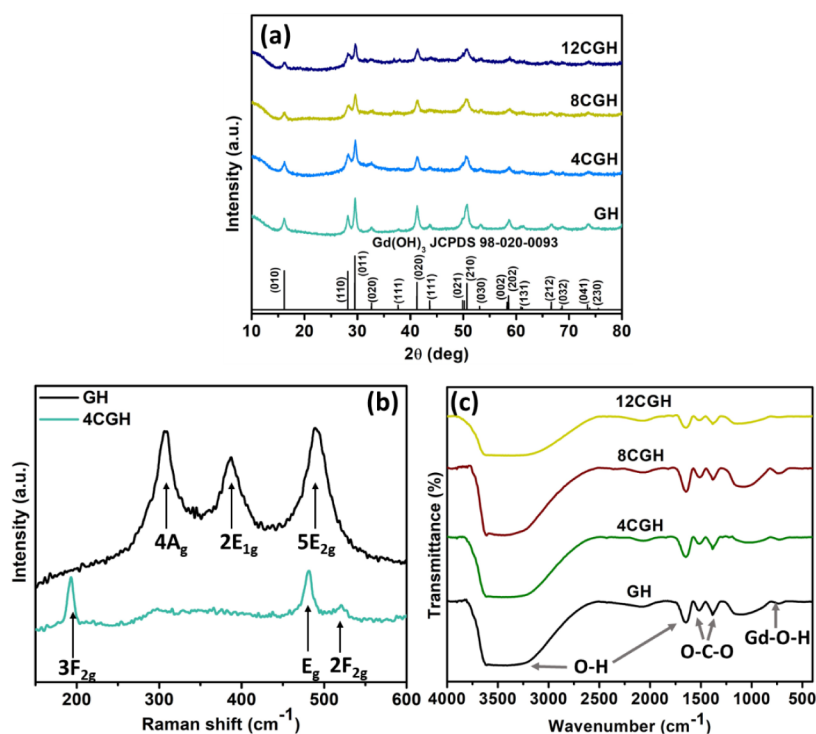
Figure 1. (a) XRD patterns; (b) Raman; and (c) FTIR spectra of GH, GH4, GH8, and 12CGH NRs.

percentage photocatalytic degradation of pollutants

$$= \frac{(A - B)}{A} \times 100\% \quad (1)$$

where A is the absorbance of 4-NP or BG only and B is the absorbance of 4-NP or BG solution after the photocatalytic degradation reaction with the respective photocatalyst.

Furthermore, the photocatalytic activity of GH and CGH NRs against 4-NP and BG was studied by applying the pseudo-first-order reactions (eq 2):

$$\ln \frac{C_0}{C} = kt \quad (2)$$

where k is the pseudo-first-order rate constant, t is the time (h), C_0 is the initial concentration of the pollutant, and C is the final concentration of the pollutant.

3. RESULTS AND DISCUSSION

3.1. Structural Properties of GH and CGH NRs. The X-ray diffraction (XRD) patterns of the microwave-assisted synthesized GH and CG NRs are presented in Figure 1a. The diffraction peaks of GH with the highest intensities were found at 2θ of 16.22°, 28.07°, 29.53°, 41.29°, and 50.69°. The diffraction pattern was matched with the hexagonal phase of GH with the $P6_3/m$ space group (JCPDS no. 98-020-0093). No significant peak shifts were observed for the CGH NRs. There is also no other phase present, suggesting that GH and CGH NRs were successfully fabricated through the micro-wave-assisted synthesis method. On the other hand, the intensity of (010), (110), and (011) planes decreased with Co^{2+} doping, which indicates a loss of crystallinity due to lattice distortion.[39]

The average crystallite size and lattice strain of GH, 4, 8, and 12CGH NRs were estimated using eqs 3 and 4, respectively, to

study the effect of doping on the structural properties of GH:[35,40]

$$D = k\lambda / \beta \cos \theta \quad (3)$$

$$\varepsilon = \frac{\beta_{hkl}}{4 \tan \theta} \quad (4)$$

where λ represents the wavelength of the X-ray, θ indicates Bragg's angle, and β is the fwhm of the specific peaks. The average crystallite size of the GH NRs was 36.00 nm. The crystallite size was reduced to 20.84 nm for 4CGH NRs and slightly increased to 21.59 nm for 8CGH NRs. However, the crystallite size decreased to 17.34 nm for 12CGH NRs (Table 2). In general, the photocatalytic activity of materials can be

Table 2. Average Crystallite Size (D, nm), Lattice Parameters (Å), Cell Volume (V_{cell}, Å³), and Average Lattice Strain (ε) of GH and CGH NRs

| sample | D (nm) | lattice parameters (Å) | | V_{cell} (Å³) | ε |
		a	c		
GH NRs	36.00	6.34	4.18	145.51	0.0012
4CGH NRs	20.84	6.33	4.18	145.05	0.0017
8CGH NRs	21.59	6.33	4.18	145.05	0.0019
12CGH NRs	17.34	6.34	4.18	145.51	0.0021

greatly affected by a reduction in crystallite size with increased doping. Smaller crystallites can result from doping, which introduces impurities that can change the crystal structure.[41,42] There are more active sites for photocatalytic reactions in smaller crystallites because they frequently have a larger surface area. However, excessive doping can lead to defects, which might enhance charge carrier separation or recombination, affecting the photocatalytic efficiency.[41,42] In contrast, the average lattice strain of the GH and CGH NRs increased with
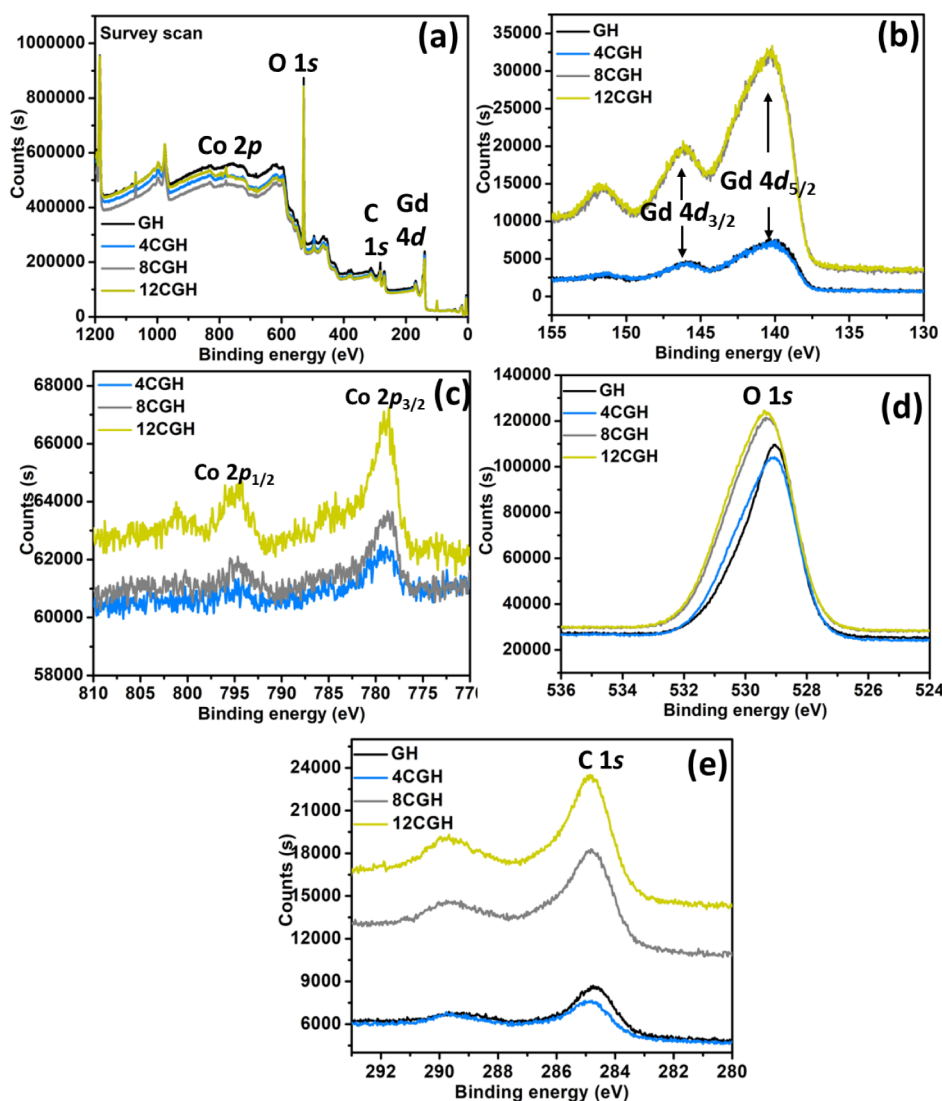
Figure 2. XPS spectra of GH and CGH NRs: (a) survey scan, (b) Gd 4d, (c) Co 2p, (d) O 1s, and (e) C 1s.

Co doping. Doping can have an impact on the lattice strain and structural properties of the crystals. The amount of dopants can lead to strains and stresses in the crystal lattice.[43] Consequently, the lattice strain increases with the increasing amount of Co^{2+}. Similar cell volumes and lattice characteristics (a and c) were found for GH with CGH NRs, indicating that the GH lattice has not been altered by Co^{2+} doping. Nonetheless, the addition of Co^{2+} ions changed the crystallite size and lattice strain of both GH and CGH NRs.

Raman spectra of GH and 4CGH NRs are displayed in Figure 1b. The three primary Raman peaks of GH were attributed to the A_g translatory (308.85 cm^{-1}), E_{2g} translatory (387.34 cm^{-1}), and E_{1g} liberation modes (490.52 cm^{-1}).[44] Those peaks are reportedly observed for the hexagonal phase of GH ($P6_3/m$) because $4A_g$, $2E_{1g}$ and $5E_{2g}$ are known to be Raman-active.[44] However, in the case of 4CGH NRs, it showed three new Raman peaks 192.91, 481.67, and 514.34 cm^{-1}, which are associated with $3F_{2g}$, E_g, and $2F_{2g}$ modes of Co^{2+} ions, respectively.[45,46] The Raman peaks of GH disappeared due to the breakdown of the lattice periodicity caused by the induced defects in the crystal lattice.[47] Figure 1c shows the FTIR spectra of GH, 4CGH, 8CGH, and 12CGH NRs. The bending vibration of Gd−O−H is responsible for

the band in the 600−750 cm^{-1} range. GH frequently exhibits peaks in the 1370−1530 cm^{-1} range, which corresponds to both symmetric and asymmetric stretching of O−C−O.[48] This can be attributed to CO_3^{2-} anions, which are commonly absorbed from the environment, made possible by the high surface area to volume ratio of the synthesized materials.[49] The absorption band at 1600 cm^{-1} is assigned to the O−H vibration in absorbed water on the sample surface. The bending and stretching of the O−H vibration of GH and 4, 8, and 12CGH were also observed at about 3550 cm^{-1}.[44]

The chemical state and electronic structure of the elements in GH, 4CGH, 8CGH, and 12CGH NRs were examined by using XPS (Figure 2). The full survey scan spectra of the materials, which confirmed the presence of Gd 4d, O 1s, and Co 2p, are shown in Figure 2a. Figure 2b displays the peak of the Gd 4d core level. Two prominent peaks were observed at approximately 140.3 and 146.1 eV, which are associated with Gd^{3+} 4$d_{3/2}$ and Gd^{3+} 4$d_{5/2}$, respectively.[50] No significant shift was observed for all of the samples. Figure 2c shows the XPS spectrum of Co 2p of 4CGH, 8CGH, and 12CGH NRs. It can be observed that 4CGH shows a lower Co 2p signal than 8CGH and 12CGH NRs. Nevertheless, two peaks were observed at ∼778.8 and 795.1 eV corresponding to Co 2$p_{1/2}$

and Co $2p_{3/2}$, respectively.[51] The energy separation between Co $2p_{1/2}$ and Co $2p_{3/2}$ for all samples was about 16 eV, which is characteristic of Co^{2+}.[52]

Figure 2d shows the XPS spectrum of the O 1s sample, where each sample has a single main peak. The OH^- anion, which is a nucleophilic oxygen species, is represented by the peak at about 529.0 eV.[53] In comparison to GH, CGH NRs showed minor changes in peak position and intensity. This might be due to the lattice distortions resulting from ionic size imbalance, which increases bond strain around oxygen atoms and raises the chemical potential.[54]

The typical C 1s peaks at 284.8 eV were observed in the spectra (Figure 2e). Therefore, the Co^{2+} ion doping has influenced the intensity of the XPS peaks, which suggests the successful incorporation of Co^{2+} ions.

3.2. Optical Properties of GH and CGH NRs. UV−vis DRS spectroscopy is a useful technique for investigating the optical properties of the synthesized GH and CGH NRs. GH is an indirect band gap semiconductor, similar to other rare earth hydroxides and some related oxide materials. This is because the conduction band minimum and valence band maximum occur at different k-points, requiring phonon involvement in electronic transitions.[55] Therefore, a Tauc plot was obtained using the Kubelka−Munk equation (eq 5) and used for the estimation of band gap energy of GH, 4CGH, 8CGH, and 12CGH NRs (Figure 3) and the UV−vis DRS spectrum of the materials is shown in Figure S1.

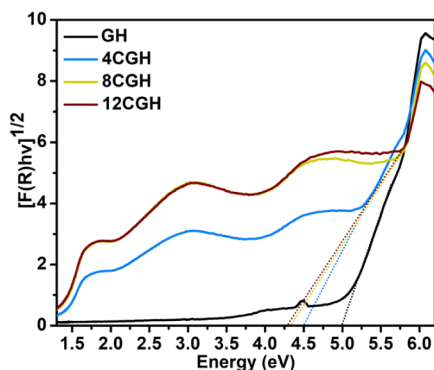$$F(R) = \left(\frac{(1-R)^2}{2R} \times h\nu \right)^{1/2}$$

(5)

Figure 3. Tauc plot obtained from the Kubelka−Munk function for the band gap energy estimation of GH and 4, 8, and 12CGH NRs.

where R is the measured absolute reflectance of the samples. The band gap energy was determined from the plots of $[F(R) h\nu]^{1/2}$ versus $h\nu$.

The band gap energy of GH was determined to be 5.00 eV, and the value decreased as Co^{2+} was incorporated into the lattice. The band gap energies of 4CGH, 8CGH, and 12CGH were 4.50, 4.31, and 4.29 eV, respectively. This shows that the incorporation of Co^{2+} can significantly reduce the band gap of the GH NRs. In general, doping modifies the electronic structure, either by creating intermediate states within the band gap or shifting the absorption edge, which can result in a more efficient use of UV light energy.[56−58] This allows the material to absorb photons with slightly lower energy or facilitates the faster generation of charge carriers. Additionally, a decrease in electron−hole pair recombination rates increases the amount

of energy from UV photons that are utilized for photocatalytic activities.[56−58]

3.3. Morphological Studies of GH and CGH NRs Using TEM. The TEM images and SAED patterns of GH, 4CGH, and 12CGH are shown in Figure 4. All of the samples were found to have rod-like features. The average length of the GH nanorods was 39 nm, and the average diameter was 12 nm, as shown in Figure 4a$_1$. Figure 4b$_1$ reveals the TEM picture of 4CGH NRs, which have an average diameter of 8 nm and a length of 59 nm. An elongation of the particle was observed upon the incorporation of 4% Co into GH. However, the diameter of 4CGH NRs decreased slightly. The diameter of the 8CGH particle remained the same, while the particle length increased slightly to 61 nm (Figure 4c$_1$). Moreover, the particle size was further increased when 12% Co was incorporated (Figure 4d$_1$), which showed an average length of 67 nm and a diameter of 10 nm. The average particle sizes of GH, 4CGH, and 12CGH NRs were tabulated in Table 3. The particle size distribution of each material is shown in Figure S2. The growth process of GH and CGH NRs involves nucleation and aggregation growth to produce the nanorod shape.[16] Generally, 1D nanorods are formed from 0D in the presence of OH^- ions and the nanorods continue to grow under the influence of many factors such as precursor pH, temperature, and reaction.[16] In this work, GH and CGH NRs were synthesized using NaOH. The OH^- from NaOH may act as a growth director to produce rod-like morphology. In addition to that, it also lowers the solution's surface tension, which prevents the nanorods from agglomeration.[49]

Also, as can be observed in Figure 4a$_2$−d$_2$, SAED analysis was used to evaluate the phase, crystallinity, and crystal orientations of GH, 4CGH, and 12CGH NRs. GH, 4CGH, and 12CGH NRs were found to exhibit four broad rings ((110), (011), (020), and (030) reflections), which are due to the hexagonal GH ($P6_3/m$) structure. Meanwhile, 8CGH displayed three prominent rings, which were also related to the (110), (011), and (030) reflections. This is in accordance with the XRD results as discussed earlier, which suggests the successful synthesis of GH and CGH NRs.

4. UV LIGHT-ASSISTED PHOTOCATALYTIC ACTIVITIES OF GH AND CGH NRS

4.1. Photocatalytic Degradation of 4-Nitrophenol. The photocatalytic degradation of 4-NP utilizing GH and CGH NRs is depicted in Figure 5a,b with respect to the average percentage and $\ln(C_0/C)$ of the photocatalytic reaction, respectively. GH and CGH NRs were used to photocatalytically degrade 4-NP under UV light irradiation. The absorbance of the solution was monitored every hour for 5 h to monitor the progress of the reaction (Figure S3). To ensure the repeatability of the findings, all experiments were carried out three times.

When the materials were irradiated with UV light, a gradual increase in the percentage degradation of 4-NP was observed with time, especially for the CGH NRs. After 5 h of UV light illumination, 12CGH NRs showed the highest photocatalytic degradation of 4-NP in which it successfully degraded 78.90 ± 4.46% of 4-NP (Figure 5a and Table S1). GH NRs showed the lowest photocatalytic activity of 62.74 ± 2.43%. The results showed that the photocatalytic activity improved with an increase in Co^{2+} doping.

The band gap energy of GH was lowered by incorporating more Co^{2+} into the GH lattice. Section 3.4 reports that the
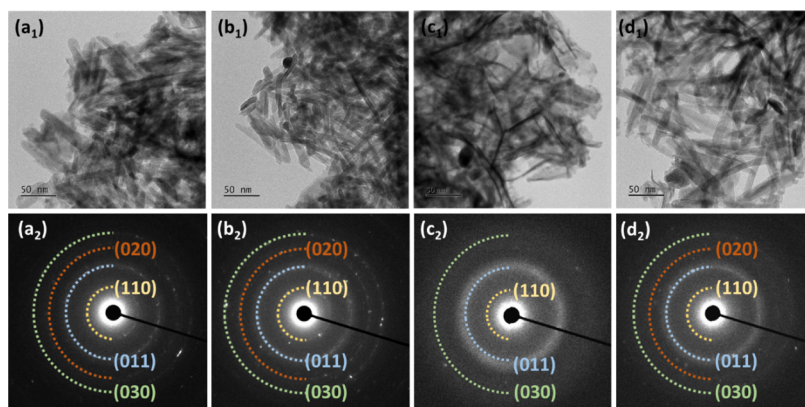
Figure 4. TEM images of (a_1) GH, (b_1) 4CGH, (c_1) 8CGH, (d_1) 12CGH, and SAED patterns of (a_2) GH, (b_2) 4CGH, (c_2) 8CGH, and (d_2) 12CGH.

Table 3. Average Particle Size from TEM Images of GH and CGH NRs (*L = Length, D = Diameter)

sample	average particle size from TEM (nm)
GH NRs	39 (L), 12 (D)
4CGH NRs	59 (L), 8 (D)
8CGH NRs	61 (L), 8 (D)
12CGH NRs	67 (L), 10 (D)

band gap energies of GH and 4, 8, and 12CGH NRs were found to be 5.00, 4.50, 4.31, and 4.29 eV, respectively. The enhanced photocatalytic degradation of 4-NP employing 12CGH NRs could be attributed to its decreased band gap energy (4.29 eV). In 12CGH NRs, e^- and h^+ were produced more efficiently than in GH.

Furthermore, the photocatalytic activity of GH and CGH NRs against 4-NP was found to follow pseudo-first-order reactions (eq 2). First-order (K) rate constants are represented in terms of 1/h. The pseudo-first-order kinetic reactions of the photocatalytic 4-NP activity degradation of GH and CGH NRs are shown in Figure 5b. GH, 4CGH, 8CGH, and 12CGH NRs were shown to have rate constants of 0.1937, 0.2091, 0.2246, and 0.2426 h^{-1}, respectively. Reaction rate constants for 12CGH NRs were found to be the highest.

4.2. Photocatalytic Degradation of BG. Figure 6a shows the photocatalytic activity of GH and CGH NRs in degrading the BG dye under UV light irradiation. The photocatalytic experiments were carried out for 5 h, and their progress was monitored by measuring the absorbance of the treated aqueous

BG dye solution using a UV−vis spectrophotometer every 1 h (Figure S3). The experiments were also conducted in triplicates.

When irradiated with UV light, GH NRs showed the lowest response among the synthesized materials. In the first hour, no response was detected from GH NRs and the response slowly increased with time. At the fifth hour, GH NRs were only able to degrade about 31% (Table S1). This response was expected, as no effect of Co doping was observed. When 4% Co was incorporated into GH, the photocatalytic response was enhanced. In the first hour, the photocatalytic response was enhanced by 36% compared to that of GH NRs. At the end of the photocatalytic experiment, 4CGH NRs showed about 61% degradation, which was almost twice as good as that of GH NRs. Increasing the Co doping to 8% resulted in about 90% of the BG dye being degraded. However, a further increase in doping showed no improvement in the photocatalytic degradation as shown for 12CGH NRs.

The low photocatalytic activity of GH NRs might be due to the reduced formation of $^\bullet$OH radicals upon exposure to UV light.[59] Its wide band gap and the concentration of BG dye might hinder the materials from absorbing light efficiently, thus producing less photogenerated e^- and h^+.[60] Upon doping, the photocatalytic activity of CGH NRs was enhanced. Their band gap energies were reduced from 4.50 to 4.29 eV, allowing the materials to absorb more light and photogenerate e^- and h^+. In the case of 8CGH, its photocatalytic degradation activity was the highest (90.10 ± 2.93%). The efficient generation of the
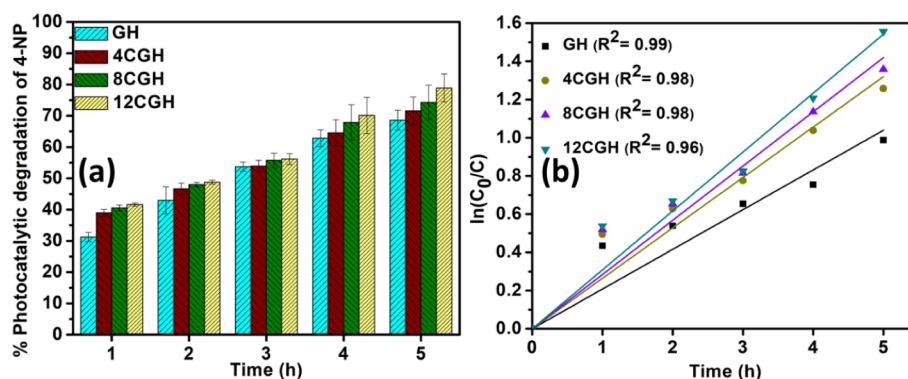

Figure 5. (a) Average percentage and (b) $\ln(C_0/C)$ plot of photocatalytic degradation of 4-NP using GH and CGH NRs under UV light irradiation.
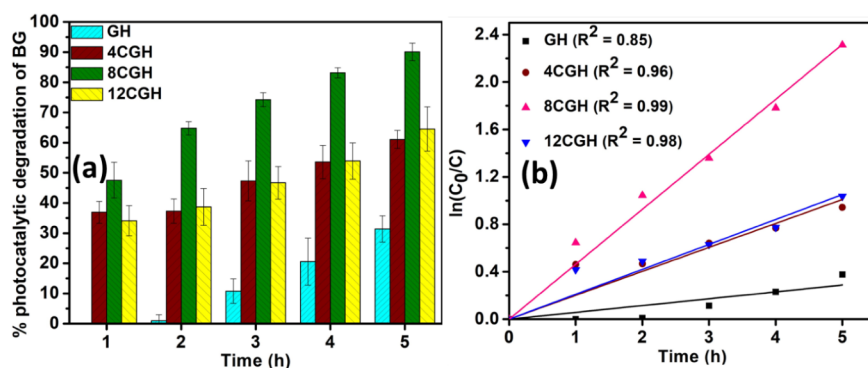
Figure 6. (a) Average percentage and (b) $\ln(C_0/C)$ plot of the photocatalytic degradation of BG using GH and CGH NRs under UV light irradiation.
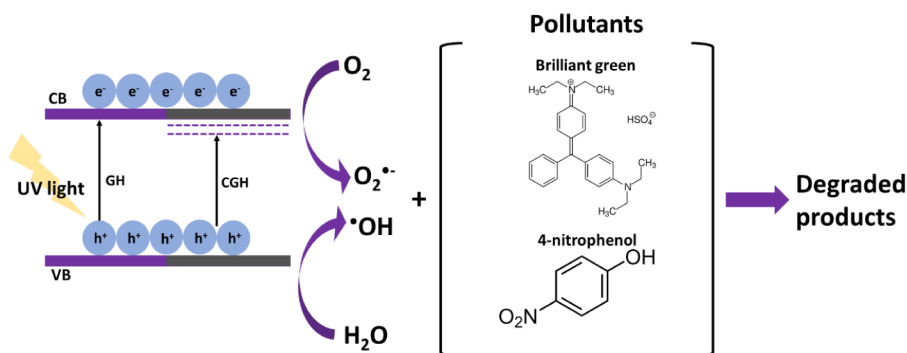

Figure 7. General mechanism of photocatalytic degradation of 4-NP and BG using GH and CGH NRs.

$O_2^{\bullet-}$ and $^\bullet OH$ radicals might be involved in the improvement of the photocatalytic degradation of BG.

Moreover, the kinetics of the photocatalytic degradation of BG using GH and CGH NRs was also found to follow the pseudo-first-order reactions (eq 2). The pseudo-first-order kinetic reactions of the photocatalytic BG activity degradation of GH and CGH NRs are shown in Figure 6b. GH, 4CGH, 8CGH, and 12CGH NRs were shown to have kinetic rate constants of 0.0575, 0.2019, 0.4636, and 0.2102 h^{-1}, respectively. Among the materials, it was found that 8CGH NRs showed the highest reaction rate constant, and GH showed the lowest reaction rate constant.

Based on the above discussion, 12CGH NRs showed the highest photocatalytic degradation of 4-NP, while 8CGH showed the best response in the photocatalytic degradation of BG. The interaction of GH and CGH with the different components of 4-NP and BG might be the reason for the optimum Co doping. Moreover, the main radicals involved in the photocatalytic degradation of 4-NP and BG might be different. In the literature, $^\bullet OH$ radicals are mainly involved in the photocatalytic degradation of 4-NP, while $O_2^{\bullet-}$ radicals are involved in the photocatalytic degradation of BG.[24,60,61] Therefore, in this study, 12CGH NRs might have produced more $^\bullet OH$ radicals and 8CGH might produce $O_2^{\bullet-}$ radicals, which are responsible for the respective performance.

4.3. General Mechanism for the Photocatalytic Degradation Activities. In general, when the material is exposed to UV light irradiation, e^- and h^+ are generated. Photogenerated e^- and h^+ react with surface O_2 and H_2O to produce $O_2^{\bullet-}$ and $^\bullet OH$ radicals, respectively. These radicals would react with pollutants, which in this case are BG and 4-NP. In the photocatalytic degradation of 4-NP, $^\bullet OH$ radicals

are reported to play an important role.[60,61] In the literature, H_2O_2 was added to the reaction mixture to provide more $^\bullet OH$ radicals. However, in this study, no H_2O_2 was added to the reaction. This suggests that the materials alone could provide $^\bullet OH$ radicals. Despite that, $O_2^{\bullet-}$ is also involved in the reaction as suggested by Kang et al.[62] Similarly, in the photocatalytic degradation of BG, the involvement of $^\bullet OH$ and the $^\bullet OH$ and $O_2^{\bullet-}$ radicals improved the photocatalytic activity. The effectiveness in the generation of e^- and h^+ upon irradiation with UV light is important in photocatalysis. In the literature, $O_2^{\bullet-}$ radicals are mainly responsible for degrading dye solutions.[24] Figure 7 illustrates the general mechanism of the photocatalytic degradation of BG and 4-NP.

It is worth noting that doping with either transition metals or nonmetals introduces intermediate energy levels inside the bandgap, allowing electron excitation to the conduction band with reduced energy. This modification increases the reactivity of the material at different UV wavelengths and improves its absorption of UV light.[63] Furthermore, by lowering the recombination rates and improving the separation of photo-generated electron−hole pairs, doping can provide shallow or deep traps for electrons or holes, increasing the photocatalytic efficiency. Additionally, even with a high bandgap, doping can optimize the material's effectiveness under UV light exposure by shifting the absorption threshold into more accessible UV regions.[64,65] Other than that, surface states, defect levels, or localized states within the band gap may act as intermediate energy levels that facilitate photon absorption and subsequent excitation at lower energies than the observed band gap energy.[66]

With this consideration, in a previous study using Ni−Gd(OH)₃, the degradation efficiencies for BG and 4-NP were

reported at 92% and 69%, respectively.[38] In contrast, CGH achieved comparable degradation for BG at 90% and a significantly higher photocatalytic degradation activity for 4-NP at 78%. This enhanced degradation of 4-NP with Co doping suggests that Co^{2+} plays a key role in improving electron−hole separation, which is critical for pollutant breakdown.[56−58] Such improvements may result from Co-induced modifications in the band structure, which facilitate more efficient electron transfer and light absorption.[64,65] This underlines the potential of Co doping in optimizing photocatalytic degradation processes, making it a promising method for environmental remediation applications.

5. CONCLUSIONS

In this study, the optical, morphological, and structural properties of microwave-assisted synthesized GH and CGH NRs were explored. XRD confirmed the formation of hexagonal GH and CGH with average crystallite sizes between 17 and 36 nm. Moreover, Raman and FT-IR analyses confirmed the presence of the vibrational modes of GH and CGH. GH and CGH NRs showed a decrease in band gap energy with Co doping, with band gap energy values decreasing from 5.00 to 4.29 eV. TEM images showed nanorod-shaped particles for all the synthesized materials, and Co^{2+} doping resulted in increased particle sizes. Under UV light irradiation, photocatalytic degradations of 4-NP and BG were also carried out. It was found that 12CGH NRs showed the greatest response in the photocatalytic degradation of 4-NP, whereas 8CGH NRs showed the best response in the degradation of BG. The efficient pollutant degradation under UV light highlights the potential of GH and CGH for water and air purification, self-cleaning surfaces, and solar-driven energy applications, advancing pollution control and sustainable energy solutions.

■ ASSOCIATED CONTENT

Data Availability Statement

All data generated or analyzed during this study are included in this article and its Supporting Information file.

Ⓢ Supporting Information

The Supporting Information is available free of charge at https://pubs.acs.org/doi/10.1021/acsomega.4c09351.

> The UV−vis absorbance spectra of $Gd(OH)_3$, 4CGH, 8CGH, and 12CGH NRs (Figure S1); the distribution of length and diameter of $Gd(OH)_3$, 4CGH, 8CGH, and 12CGH NRs (Figure S2); UV−vis absorption spectra of 4-NP in the presence of GH and CGH NRs under UV light irradiation (Figure S3); UV−vis absorption spectra of BG in the presence of GH and CGH NRs under UV light irradiation (Figure S4); the average percentage of photocatalytic activities of GH and CGH NRs for 4-NP and BG degradation under UV light irradiation (Table S1) (PDF)

■ AUTHOR INFORMATION

Corresponding Author

> **Mohammad Mansoob Khan** − *Chemical Sciences, Faculty of Science, Universiti Brunei Darussalam, Gadong BE 1410, Brunei Darussalam;* ● orcid.org/0000-0002-8633-7493; Email: mmansoobkhan@yahoo.com, mansoob.khan@ubd.edu.bn

Authors

> **Shaidatul Najihah Matussin** − *Chemical Sciences, Faculty of Science, Universiti Brunei Darussalam, Gadong BE 1410, Brunei Darussalam*
> **Fazlurrahman Khan** − *Ocean and Fisheries Development International Cooperation Institute, Pukyong National University, Busan 48513, Republic of Korea; Marine Integrated Biomedical Technology Center, The National Key Research Institutes in Universities and Research Center for Marine Integrated Bionics Technology, Pukyong National University, Busan 48513, Republic of Korea;* ● orcid.org/0000-0002-4902-3188
> **Mohammad Hilni Harunsani** − *Chemical Sciences, Faculty of Science, Universiti Brunei Darussalam, Gadong BE 1410, Brunei Darussalam*
> **Young-Mog Kim** − *Marine Integrated Biomedical Technology Center, The National Key Research Institutes in Universities, Research Center for Marine Integrated Bionics Technology, and Department of Food Science and Technology, Pukyong National University, Busan 48513, Republic of Korea;* ● orcid.org/0000-0002-2465-8013

Complete contact information is available at:
https://pubs.acs.org/10.1021/acsomega.4c09351

Author Contributions

S.N.M.: Methodology; Investigation, Data Curation; Writing − Original Draft. F.K.: Data Curation, Formal Analysis. M.H.H.: Supervision, Writing − Review and Editing. Y.-M.K.: Resources, Formal Analysis. M.M.K.: Supervision, Conceptualization, Funding Acquisition, Writing − Review and Editing.

Notes

The authors declare no competing financial interest.

■ ACKNOWLEDGMENTS

■ REFERENCES

(1) Khan, I.; Saeed, K.; Khan, I. Nanoparticles: Properties, Applications and Toxicities. *Arabian J. Chem.* **2019**, *12*, 908−931.

(2) Gupta, R.; Chauhan, H.; Garg, V. K.; Kataria, N. Chemical and Physical Properties of Nanoparticles and Hybrid Materials. In *Sustainable Nanotechnology for Environmental Remediation*; Elsevier, 2022, pp. 199−220. DOI: .

(3) Matussin, S. N.; Harunsani, M. H.; Khan, M. M. CeO2 and CeO2-Based Nanomaterials for Photocatalytic, Antioxidant and Antimicrobial Activities. *J. Rare Earths* **2023**, *41* (2), 167−181.

(4) Matussin, S. N.; Khan, F.; Harunsani, M. H.; Kim, Y.-M.; Khan, M. M. Effect of Pd-Doping Concentrations on the Photocatalytic, Photoelectrochemical, and Photoantibacterial Properties of CeO2. *Catalysts* **2023**, *13* (1), 96.

(5) Matussin, S. N.; Khan, F.; Chandika, P.; Harunsani, M. H.; Ahmad, N.; Kim, Y. M.; Jung, W. K.; Khan, M. M. Effects of NO3−, Cl−, and CH3COO− Anions and Diethylene Glycol on the Morphological, Structural, Antidiabetic, and Cell Viability Properties of CeO2 Nanoparticles. *RSC Adv.* **2023**, *13* (23), 15421−15436.

(6) Sternik, M.; Wdowik, U. D. Probing the impact of magnetic interactions on the lattice dynamics of two-dimensional Ti2X (X = C, N) MXenes. *Phys. Chem. Chem. Phys.* **2018**, *20* (11), 7754−7763.

(7) Matussin, S. N.; Rahman, A.; Khan, M. M. Role of Anions in the Synthesis and Crystal Growth of Selected Semiconductors. *Front. Chem.* **2022**, *10*, 10.

(8) Khan, M. M.; Matussin, S. N. Sm $_2$ O $_3$ and Sm $_2$ O $_3$ -Based Nanostructures for Photocatalysis, Sensors, CO Conversion, and Biological Applications. *Catal. Sci. Technol.* **2023**, *13*, 2274.

(9) Matussin, S. N.; Harunsani, M. H.; Khan, M. M. Eu(OH)3 and Eu(OH)3-Based Nanostructures: Synthesis, Properties, and Uses. *Mater. Today Commun.* **2024**, *39*, 108775.

(10) Matussin, S. N.; Khan, F.; Harunsani, M. H.; Kim, Y.-M.; Khan, M. M. Impact of Co-Doping on the Visible Light-Driven Photocatalytic and Photoelectrochemical Activities of Eu(OH) $_3$. *ACS Omega* **2024**, *9* (14), 16420−16428.

(11) Liang, S.; Wang, H.; Li, Y.; Qin, H.; Luo, Z.; Huang, B.; Zhao, X.; Zhao, C.; Chen, L. Rare-Earth Based Nanomaterials and Their Composites as Electrode Materials for High Performance Supercapacitors: A Review. *Sustain. Energy Fuels* **2020**, *4* (8), 3825−3847.

(12) Fu, R.; Ou, M.; Yang, C.; Hu, Y.; Yin, H. Enhanced Luminescence and Paramagnetic Properties of Gd2O3: Tb3+ Multifunctional Nanoparticles by K+/Co2+ Doping. *J. Lumin.* **2020**, *222* (2019), 117154.

(13) Singh, P.; Kachhap, S.; Singh, P.; Singh, S. K. Lanthanide-Based Hybrid Nanostructures: Classification, Synthesis, Optical Properties, and Multifunctional Applications. *Coord. Chem. Rev.* **2022**, *472*, 214795.

(14) Qiu, X.; Xu, J.; Cardoso Dos Santos, M.; Hildebrandt, N. Multiplexed Biosensing and Bioimaging Using Lanthanide-Based Time-Gated Förster Resonance Energy Transfer. *Acc. Chem. Res.* **2022**, *55* (4), 551−564.

(15) Mu, Q.; Wang, Y. A Simple Method to Prepare Ln(OH)3 (Ln = La, Sm, Tb, Eu, and Gd) Nanorods Using CTAB Micelle Solution and Their Room Temperature Photoluminescence Properties. *J. Alloys Compd.* **2011**, *509* (5), 2060−2065.

(16) Ji, X.; Hu, P.; Li, X.; Zhang, L.; Sun, J. Hydrothermal Control, Characterization, Growth Mechanism, and Photoluminescence Properties of Highly Crystalline 1D Eu(OH)3nanostructures. *RSC Adv.* **2020**, *10* (55), 33499−33508.

(17) Shih, K. Y.; Yu, S. C. Microwave-Assisted Rapid Synthesis of Eu(Oh)3/Rgo Nanocomposites and Enhancement of Their Antibacterial Activity against *Escherichia Coli*. *Materials* **2022**, *15* (1), 43.

(18) Lee, D.; Seo, J.; Valladares, L. D. L. S.; Avalos Quispe, O.; Barnes, C. H. W. Magnetic and Structural Properties of Yellow Europium Oxide Compound and Eu(OH)3. *J. Solid State Chem.* **2015**, *228*, 141−145.

(19) Kumar Padhi, D.; Pradhan, G. K.; Parida, K. M.; Singh, S. K. Facile Fabrication of Gd(OH)3 Nanorod/RGO Composite: Synthesis, Characterisation and Photocatalytic Reduction of Cr(VI). *Chem. Eng. J.* **2014**, *255*, 78−88.

(20) Matussin, S. N.; Harunsani, M. H.; Khan, M. M. Gd(OH)3 and Gd(OH)3-Based Heterostructures: Synthesis and Their Photocatalytic, Drug Delivery, Contrast Agents, and Toxicity Studies. *J. Rare Earths*, **2024**.

(21) Xu, Y.; Goyanes, A.; Wang, Y.; Weston, A. J.; So, P. W.; Geraldes, C. F. G. C.; Fogg, A. M.; Basit, A. W.; Williams, G. R. Layered Gadolinium Hydroxides for Simultaneous Drug Delivery and Imaging. *Dalton Trans.* **2018**, *47* (9), 3166−3177.

(22) Shao, B.; Zhang, X.; Guo, A.; Jiang, L.; Cui, F.; Yang, X. Eu3+-Doped Layered Gadolinium Hydroxides as Drug Carriers and Their Bactericidal Behavior. *Mater. Sci. Eng.* **2021**, *127*, 112213.

(23) Kobayashi, Y.; Morimoto, H.; Nakagawa, T.; Kubota, Y.; Gonda, K.; Ohuchi, N. Fabrication of Gadolinium Hydroxide Nanoparticles Using Ion-Exchange Resin and Their MRI Property. *J. Asian Ceram. Soc.* **2016**, *4* (1), 138−142.

(24) Liu, W.; Yang, Z.; Zou, B.; Liao, W.; Wang, Y.; Wang, C.; Li, S.; Niu, X. The Photocatalytic Application of Gd(OH)3/Cd0.8Zn0.2S Nanocomposites in U(VI) Reduction. *Chem. Eng. J.* **2023**, *466*, 143117.

(25) Li, J.; Cai, H.; Dong, S.; Zhang, T.; Peng, C.; Shi, X.; Shen, M. A Facile Synthesis of Size- and Shape-Controlled Gd(OH)3 Nanoparticles and Gd(OH)3@Au Core/Shell Nanostars. *New J. Chem.* **2017**, *41* (24), 15136−15143.

(26) Du, Y.; Xing, M.; Li, Z.; Guo, W. PEGylated Gd(OH)3 Nanorods as Metabolizable Contrast Agents for Computed Tomography Imaging. *New J. Chem.* **2015**, *39* (11), 8999−9005.

(27) Huang, S.; Liu, J.; Liu, D.; Yuan, Q. Facile and Large-Scale Synthesis of Gd(OH)3 Nanorods for MR Imaging with Low Toxicity. *New J. Chem.* **2012**, *36* (6), 1335.

(28) Al-Mhyawi, S. R.; Abdel Salam, M. Enhancement of Photocatalytic Activity of Gd(OH)3 Nanoparticles by Pd Deposition for Reduction of CO2 to Methanol. *J. Photochem. Photobiol., A* **2018**, *367*, 89−93.

(29) Singh, V.; Naka, T.; Takami, S.; Sahraneshin, A.; Togashi, T.; Aoki, N.; Hojo, D.; Arita, T.; Adschiri, T. Hydrothermal Synthesis of Inorganic-Organic Hybrid Gadolinium Hydroxide Nanoclusters with Controlled Size and Morphology. *Dalton Trans.* **2013**, *42* (45), 16176−16184.

(30) Li, G.; Liang, Y.; Zhang, M.; Yu, D. Size-Tunable Synthesis and Luminescent Properties of Gd(OH) 3: Eu3+ and Gd2O3: Eu3+ Hexagonal Nano-/Microprisms. *CrystEngcomm* **2014**, *16* (29), 6670−6679.

(31) Zong, Y.; Feng, J.; Sun, Y.; Li, X.; Bai, J.; Zheng, X. Hydrothermal Synthesis of Uniform Fe-Doped Gd(OH)3 Nanorods and Their Magnetic Properties: Phase Conversion from Paramagnetism to Ferromagnetism. *Ceram. Int.* **2017**, *43* (10), 7881−7888.

(32) Chiu, Y.-H.; Chang, T.-F.; Chen, C.-Y.; Sone, M.; Hsu, Y.-J. Mechanistic Insights into Photodegradation of Organic Dyes Using Heterostructure Photocatalysts. *Catalysts* **2019**, *9* (5), 430.

(33) Thambiraj, S.; Sharmila, G.; Ravi Shankaran, D. Green Adsorbents from Solid Wastes for Water Purification Application. *Mater. Today: proc.* **2018**, *5* (8), 16675−16683.

(34) Daneshvar, N.; Salari, D.; Khataee, A. R. Photocatalytic Degradation of Azo Dye Acid Red 14 in Water: Investigation of the Effect of Operational Parameters. *J. Photochem. Photobiol., A* **2003**, *157* (1), 111−116.

(35) Matussin, S. N.; Harunsani, M. H.; Tan, A. L.; Cho, M. H.; Khan, M. M. Effect of Co2+ and Ni2+ Co-Doping on SnO2 Synthesized via Phytogenic Method for Photoantioxidant Studies and Photoconversion of 4-Nitrophenol. *Mater. Today Commun.* **2020**, *25* (September), 101677.

(36) Liu, S.; Cai, Y.; Cai, X.; Li, H.; Zhang, F.; Mu, Q.; Liu, Y.; Wang, Y. Catalytic Photodegradation of Congo Red in Aqueous Solution by Ln(OH) 3 (Ln = Nd, Sm, Eu, Gd, Tb, and Dy) Nanorods. *Appl. Catal., A* **2013**, *453*, 45−53.

(37) González, C. M. O.; Morales, E. M. C.; Tellez, A. D. M. N.; Quezada, T. E. S.; Kharissova, O. V.; Méndez-Rojas, M. A. CO2 Capture by MOFs. In *Handbook of Greener Synthesis of Nanomaterials and Compounds*; Elsevier, 2021, pp. 407−448. DOI: .

(38) Matussin, S. N.; Khan, F.; Harunsani, M. H.; Kim, Y.-M.; Khan, M. M. Photocatalytic Degradation of Brilliant Green and 4-Nitrophenol Using Ni-Doped Gd(OH)3 Nanorods. *Sci. Rep.* **2024**, *14* (1), 8269.

(39) Pal, M.; Pal, U.; Jiménez, J. M. G. Y.; Pérez-Rodríguez, F. Effects of Crystallization and Dopant Concentration on the Emission Behavior of TiO2: Eu Nanophosphors. *Nanoscale Res. Lett.* **2012**, *7* (1), 1.

(40) Matussin, S. N.; Tan, A. L.; Harunsani, M. H.; Cho, M. H.; Khan, M. M. Green and Phytogenic Fabrication of Co-Doped SnO2 Using Aqueous Leaf Extract of Tradescantia Spathacea for Photoantioxidant and Photocatalytic Studies. *Bionanoscience* **2021**, *11* (1), 120−135.

(41) Krishnakumar, V.; Boobas, S.; Jayaprakash, J.; Rajaboopathi, M.; Han, B.; Louhi-Kultanen, M. Effect of Cu Doping on TiO2 Nanoparticles and Its Photocatalytic Activity under Visible Light. *J. Mater. Sci.: Mater. Electron.* **2016**, *27* (7), 7438−7447.

(42) Ashokkumar, M.; Rajkumar, M.; Pugazhvadivu, K. S. Assessment of Properties, Photocatalytic Activity, Cytotoxicity, and

Antibacterial Activity of (Cu, Cr) Dual-Doped ZnO Nanoparticles. *J. Inorg. Organomet. Polym. Mater.* **2023**, *33* (9), 2974−2983.

(43) Grushka, O. G.; Gorlei, P. M.; Bestsennyi, A. V.; Grushka, Z. M. Effect of Doping with Gadolinium on the Physical Properties of Hg3In2Te6. *Semiconductors* **2000**, *34* (10), 1147−1150.

(44) Kang, J. G.; Min, B. K.; Sohn, Y. Synthesis and Characterization of Gd(OH)3 and Gd2O3 Nanorods. *Ceram. Int.* **2015**, *41* (1), 1243−1248.

(45) UmaSudharshini, A.; Bououdina, M.; Venkateshwarlu, M.; Dhamodharan, P.; Manoharan, C. Solvothermal Synthesis of Cu-Doped Co3O4 Nanosheets at Low Reaction Temperature for Potential Supercapacitor Applications. *Appl. Phys. A* **2021**, *127* (5), 353.

(46) Wang, Y.; Wei, X.; Hu, X.; Zhou, W.; Zhao, Y. Effect of Formic Acid Treatment on the Structure and Catalytic Activity of Co 3 O 4 for N 2 O Decomposition. *Catal. Lett.* **2019**, *149* (4), 1026−1036.

(47) Komaraiah, D.; Radha, E.; James, J.; Kalarikkal, N.; Sivakumar, J.; Ramana Reddy, M. V.; Sayanna, R. Effect of Particle Size and Dopant Concentration on the Raman and the Photoluminescence Spectra of TiO 2: Eu 3+ Nanophosphor Thin Films. *J. Lumin.* **2019**, *211*, 320−333.

(48) Kang, J. G.; Jung, Y.; Min, B. K.; Sohn, Y. Full Characterization of Eu(OH) 3 and Eu 2 O 3 Nanorods. *Appl. Surf. Sci.* **2014**, *314*, 158−165.

(49) Chen, F.; Zhang, X. H.; Hu, X. D.; Zhang, W.; Zeng, R.; Liu, P. D.; Zhang, H. Q. Synthesis and Characteristics of Nanorods of Gadolinium Hydroxide and Gadolinium Oxide. *J. Alloys Compd.* **2016**, *664*, 311−316.

(50) Ullah, N.; Imran, M.; Liang, K.; Yuan, C. Z.; Zeb, A.; Jiang, N.; Qazi, U. Y.; Sahar, S.; Xu, A. W. Highly Dispersed Ultra-Small Pd Nanoparticles on Gadolinium Hydroxide Nanorods for Efficient Hydrogenation Reactions. *Nanoscale* **2017**, *9* (36), 13800−13807.

(51) Matussin, S. N.; Khan, F.; Harunsani, M. H.; Kim, Y.-M.; Khan, M. M. Visible-Light-Induced Photocatalytic and Photoantibacterial Activities of Co-Doped CeO 2. *ACS Omega* **2023**, *8* (13), 11868−11879.

(52) Sutka, A.; Kaambre, T.; Parna, R.; Juhnevica, I.; Maiorov, M.; Joost, U.; Kisand, V. Co Doped ZnO Nanowires as Visible Light Photocatalysts. *Solid State Sci.* **2016**, *56*, 54−62.

(53) Jones, T. E.; Rocha, T. C. R.; Knop-Gericke, A.; Stampfl, C.; Schlögl, R.; Piccinin, S. Thermodynamic and Spectroscopic Properties of Oxygen on Silver under an Oxygen Atmosphere. *Phys. Chem. Chem. Phys.* **2015**, *17* (14), 9288−9312.

(54) Bagus, P. S.; Sousa, C.; Illas, F. Consequences of Electron Correlation for XPS Binding Energies: Representative Case for C(1s) and O(1s) XPS of CO. *J. Chem. Phys.* **2016**, *145*, 14.

(55) Zatsepin, D. A.; Boukhvalov, D. W.; Zatsepin, A. F.; Kuznetsova, Y. A.; Mashkovtsev, M. A.; Rychkov, V. N.; Shur, V. Y.; Esin, A. A.; Kurmaev, E. Z. Electronic Structure, Charge Transfer, and Intrinsic Luminescence of Gadolinium Oxide Nanoparticles: Experiment and Theory. *Appl. Surf. Sci.* **2018**, *436*, 697−707.

(56) Erfan, N. A.; Mahmoud, M. S.; Kim, H. Y.; Barakat, N. A. M. Synergistic Doping with Ag, CdO, and ZnO to Overcome Electron-Hole Recombination in TiO2 Photocatalysis for Effective Water Photo Splitting Reaction. *Front. Chem.* **2023**, *11*, 11.

(57) Madani, M.; Mansour, H.; Alonizan, N.; El Mir, L. Effect of Mg and Cu Co-Doping on Nanostructured TiO2 Photocatalytic Activity. *J. Mater. Sci.: Mater. Electron.* **2024**, *35* (17), 1168.

(58) Zhang, Q.; Wang, Y.; Jia, Y.; Yan, W.; Li, Q.; Zhou, J.; Wu, K. Engineering the Electronic Structure towards Visible Lights Photocatalysis of CaTiO3 Perovskites by Cation (La/Ce)-Anion (N/S) Co-Doping: A First-Principles Study. *Molecules* **2023**, *28* (20), 7134.

(59) Bogusz, K.; Cardillo, D.; Tehei, M.; Boutard, T.; Barker, P. J.; Devers, T.; Rosenfeld, A.; Dou, S. X.; Liu, H. K.; Konstantinov, K. Biocompatible Bi(OH)3 Nanoparticles with Reduced Photocatalytic Activity as Possible Ultraviolet Filter in Sunscreens. *Mater. Res. Bull.* **2018**, *108*, 130−141.

(60) Verma, A.; Jaihindh, D. P.; Fu, Y. P. Photocatalytic 4-Nitrophenol Degradation and Oxygen Evolution Reaction in CuO/g-C3N4 Composites Prepared by Deep Eutectic Solvent-Assisted Chlorine Doping. *Dalton Trans.* **2019**, *48* (24), 8594−8610.

(61) Fan, Y.; Wu, D.; Zhang, S.; Zhang, L.; Hu, W.; Zhu, C.; Gong, X. Effective Photodegradation of 4-Nitrophenol with CuO Nano Particles Prepared by Ionic Liquids/Water System. *Green Chem. Eng.* **2022**, *3* (1), 15−24.

(62) Kang, S.; Jang, J.; Pawar, R. C.; Ahn, S. H.; Lee, C. S. Low Temperature Fabrication of Fe2O3 Nanorod Film Coated with Ultra-Thin g-C3N4 for a Direct z-Scheme Exerting Photocatalytic Activities. *RSC Adv.* **2018**, *8* (59), 33600−33613.

(63) Piątkowska, A.; Janus, M.; Szymański, K.; Mozia, S. C-,N- and S-Doped TiO2 Photocatalysts: A Review. *Catalysts* **2021**, *11* (1), 144.

(64) Luo, Y.; Xu, Y.; Liu, X.; Xue, H.; Qian, Q.; Chen, Q. Design of Cu−Ce Co-Doped TiO2 for Improved Photocatalysis. *J. Mater. Sci.* **2017**, *52* (3), 1265−1271.

(65) Khlyustova, A.; Sirotkin, N.; Kusova, T.; Kraev, A.; Titov, V.; Agafonov, A. Doped TiO 2: The Effect of Doping Elements on Photocatalytic Activity. *Mater. Adv.* **2020**, *1* (5), 1193−1201.

(66) Xu, J.; Teng, Y.; Teng, F. Effect of Surface Defect States on Valence Band and Charge Separation and Transfer Efficiency. *Sci. Rep.* **2016**, *6* (1), 32457.